Positron Emission Tomography with Sparse Block Rings and Continuous Bed Motion

Nicolas A. Karakatsanis, *Senior Member, IEEE*, Sara A. Zein and Sadek A. Nehmeh

***Abstract*–Clinical PET systems employ compact block rings to maximize sensitivity per axial field-of-view (AFOV) length, thereby resulting in considerable manufacturing costs. To reduce the cost per AFOV length, a sparse block rings configuration is modeled on a Siemens Biograph™ mMR PET/MR scanner (sparse-mMR) by removing the coincidence counts from every other detector block ring. Moreover, Continuous Bed Motion (CBM) is performed along a limited distance to eliminate the axial sensitivity gaps. List-mode PET mMR data of the NEMA image quality phantom with 4:1 spheres-to-background ratio was acquired for 30min. The counts were binned assuming a sparse-mMR configuration and a CBM acquisition of constant speed along a distance of 2 blocks (16 detector rings, 6.4cm). The CBM scans were simulated by axially shifting the stationary mMR data to 16 different positions, including a reference, removing the counts associated with any even block rings, and shifting back to the reference position. The process was repeated with different input PET data of equal duration for all 16 positions and the corresponding output data were added. The CBM mode eliminated all axial sensitivity discontinuities by evenly acquiring data throughout the gaps. Contrast recovery (CR) and background variability (BV) were evaluated for PET images reconstructed from sparse-mMR CBM data against mMR and compact-½mMR stationary data of equal duration (~5min). The latter consisted of counts associated with only the 4 central mMR block rings. A similar CR performance was attained between the three configurations. Mean BV for sparse-mMR with CBM was 3.6% higher than mMR. Nevertheless, sparse-mMR with CBM attained a smoother axial variation in image noise, relative to compact-½mMR. CBM can restore continuity in the axial sensitivity profile of PET systems with sparse block rings to achieve similar contrast recovery and smoother noise variation, compared to compact systems, at half the cost or double the AFOV.**

I. Introduction

MODERN clinical Positron Emission Tomography (PET) scanners typically adopt a compact configuration of parallel scintillating detector block rings to attain high sensitivity per unit length of their axial field-of-view (AFOV) [1]. However, this type of ring configuration yields to the smallest possible AFOV for a given number of scintillating detector rings of fixed dimensions. In the meantime, the crystal detector block units remain the hardware component with the highest contribution to the total manufacturing cost of modern clinical PET scanners. [2]. Consequently, the state-of-the-art PET systems of today are associated with relatively high manufacturing costs per AFOV length units thereby forcing the development of clinical PET systems with limited AFOV (<26cm) to keep the manufacturing cost within an affordable range for most clinical facilities across the world. However, short AFOVs in PET systems are currently constraining the full potential of human molecular imaging as they hinder the truly simultaneous acquisition of radiotracers distribution from multiple organs and tissues that are distant to each other but may be highly associated in terms of specific molecular mechanisms, such as the brain and the heart or the heart and the abdomen [3].

The current generation of clinical PET systems typically employ extensive 3D acquisition modes to enhance the system sensitivity by accepting coincidence events across detector rings with large axial distance to enhance the system sensitivity in the center of the AFOV [4]. As a result, the signal-to-noise ratio (SNR) of the PET data at the central region of the AFOV can be increased as a function of the total number of detector rings for a given size of detector elements and ring diameter [4]. At the same time, the 3D PET system sensitivity and, thus the data SNR per transaxial slice remains moderate at the edges of the AFOV, regardless of the AFOV length. Therefore, the reduction in 3D sensitivity from the center to the edges of the AFOV becomes steeper for shorter AFOVs [5]. Thus, PET images obtained from systems with longer AFOVs are expected to suffer from a less steep SNR decrease towards the AFOV edges. This feature can be critical for ensuring uniform and reproducible quantitative accuracy and detectability performance especially in cases where the lesions location is not known a-priori or quantitative comparisons are made between lesions located in the center and the edges of the AFOV within the same scan or across a series of scans. In single-bed dynamic PET studies, the extended AFOVs can be even so important due to the overall higher levels of noise expected form the acquisition of the often-short dynamic PET frames [6].

Furthermore, truly simultaneous imaging of multiple human body organs is prevented with current AFOVs, therefore limiting the investigation of systemic molecular relationships between distant organs, such as the brain-heart [7] and brain-gut axis [8]. Besides, short AFOVs are more likely to exclude neighboring blood pool regions, such as heart ventricles and aortic or carotid arteries, which are valuable for PET kinetic modeling [9, 10].

In addition, the short AFOVs of current clinical PET systems may pose limitations to several human PET studies requiring the truly simultaneous acquisition of static or dynamic PET signal from multiple regions of the body that are distant to each other. Currently, the clinical PET systems may

Manuscript received November 30th, 2019.

N. A. Karakatsanis is with the Department of Radiology, Weill Cornell Medical College, Cornell University, New York, NY, USA, 10021 (e-mail: nak2032@med.cornell.edu)

S. A. Zein and S. A. Nehmeh are also with the Department of Radiology, Weill Cornell Medical College, Cornell University, New York, NY, USA, 10021

978-1-7281-4164-0 /19/$31.00 ©2019 IEEE

Authorized licensed use limited to: Cornell University Library. Downloaded on July 21,2020 at 23:57:56 UTC from IEEE Xplore. Restrictions apply.

attain whole-body PET scan sessions only via sequential acquisitions. Thus, the whole-body human PET studies nowadays are conducted either by continuously translating the patient table along the scanner axis, a 3D scan protocol known as continuous bed motion (CBM) mode to ensure uniform axial sensitivity across the human body [11], or by incrementally translating the bed at discrete axial positions with a considerable overlap between them to attain a nearly uniform 3D scan sensitivity across the different stationary bed positions (step-and-shoot mode) covering the total human body [1]. In both CBM and step-and-shoot mode, different AFOV regions are scanned at a given time frame, which can trigger non-negligible quantitative bias when comparing activity concentrations between distant organs especially at early post-injection scan time windows when the radiotracer spatial distribution is more likely to change between the respective scan frames. Moreover, the short AFOVs currently pose the most significant limitations for the clinical translation of whole-body dynamic PET imaging, thus hindering the transfusion of the quantitative benefits of multi-parametric 4D PET imaging in routine nuclear medicine PET exams [12-14]. Indeed, the large degree of AFOV confinement adopted by the modern human PET systems to reduce their development cost, has prevented the truly continuous spatiotemporal sampling of the radiotracers distribution across the total body [15]. Despite the recent development of clinically applicable and robust whole-body graphical analysis methods [16, 17], which have become feasible thanks to the deployment in clinical PET systems of several SNR enhancing technologies including Time-of-Flight acquisition and Point-Spread-Function (PSF) resolution modeling reconstruction algorithms [18] [19], fully compartmental kinetic modeling across multiple bed positions has not yet become feasible with limited AFOV PET systems [20-22].

In the past, to overcome the aforementioned constraints, PET scanner prototypes with long (50-140cm) or ultra-long (~2m) total-body AFOVs have been proposed with impressive results for either static or dynamic molecular imaging applications [23-26]. However, these systems rely on highly compact ring configurations, thereby requiring a very high number of detector elements to cover their long AFOV [27]. Thus, such geometries are associated with a very high cost, relative to that of conventional clinical PET systems with much fewer elements of the same scintillation detectors. Consequently, total-body PET systems with compact ring configurations have not yet attained a wide adoption in clinic [28].

In the meantime, the modern PET systems have been employing highly efficient signal readout electronics, fast scintillation and optical detectors to support very fine time-of-flight (TOF) resolutions as well as reconstruction software capable of modeling the point-spread function (PSF) resolution response of the PET scanners [29, 30]. As a result, the PET projection data SNR, and the associated reconstructed PET image quality have been tremendously improved over the recent years for a given acquisition time or administered radiotracer dosage thus benefiting lesion detectability and treatment response assessments reliability and reproducibility [31] [32, 33]. The attained PET data SNR gain has hitherto been exploited to improve the trade-off between scan time and administered dosage to enable novel application of PET molecular imaging that were not previously feasible in clinic and require either ultra-fast acquisitions e.g. to freeze motion or allow dynamic whole-body scans, or ultra-low radiotracer dosages, e.g. to reduce radiation exposure from multiple follow-up or screening exams [34, 35]. On the other hand, the PET systems AFOVs have only marginally been extended despite the obvious benefits of long AFOV 3D PET imaging. In fact, the gain attained in PET data SNR with the aforementioned recent scanner technology developments could have been partially exploited to also design sparse PET systems of reduced cost per AFOV length unit in order to enable the widespread translation of some of the unique capabilities of total-body PET imaging in routine clinical imaging exams.

Indeed, over the past two decades, a few sparse PET detector configurations were proposed to permit PET AFOV extensions at a reduced cost. Proposals included either a very large axial gap between two PET scanner gantries [36], or very small axial gaps between the transaxial detector rows of each block [37, 38]. The former configuration limited the transaxial FOV at the central gap region and triggered considerable non-uniformities across the axial sensitivity profile. The latter required the manufacturing of block detectors with equal gaps between the transaxial detector rows made of material of similar PET attenuation properties as the detector crystals. An alternative strategy addressing these limitations could be the introduction of axial gaps of a moderate size equal to that of block rings of existing PET systems. The gaps can be interleaved either between all block rings of a current PET system to extend its AFOV (Fig. 1), or between the half central block rings to reduce its cost.

With this study, we introduce a cost-effective sparse block detector rings configuration that can be adopted in a straightforward manner from a wide range of current generation clinical PET systems. The proposed sparse configuration can be implemented by uniformly interleaving axial gaps of width equal to a physical block ring between the physical block rings of an existing clinical PET system. As a result, the current AFOV can be doubled at almost no additional cost or maintained at its current length but at half the manufacturing cost. Furthermore, we employ the previously developed CBM PET scan technology for a novel purpose: to balance the 3D PET axial sensitivity between the transaxial slices corresponding to sensitive block rings and those corresponding to the interleaved axial gaps between the block rings, thus avoiding any image artifacts and large noise non-uniformities across the AFOV due to the presence of axial gaps. More specifically, we will evaluate the feasibility and performance of CBM PET acquisitions with the proposed sparse PET detector block rings configuration employing a clinical non-TOF simultaneous PET/MR scanner. NEMA image quality performance measurements of the proposed configuration will be obtained and compared against those of the original PET compact scanner and a hypothetical compact scanner consisting of only the half most-central block rings. We hypothesize that the expected discontinuities in the 3D axial sensitivity profile can be compensated by performing CBM acquisitions of constant speed over a limited axial

Authorized licensed use limited to: Cornell University Library. Downloaded on July 21,2020 at 23:57:56 UTC from IEEE Xplore. Restrictions apply.

distance such that a balanced data acquisition is attained across all axial projection planes.

II. Methods and Materials

A. Sparse PET detector block rings configuration

The proposed sparse PET block ring configuration and CBM 3D acquisition was evaluated using experimental phantom data acquired with a Siemens Biograph™ mMR PET/MR scanner at our institution. The system consists of 8 contiguous detector block rings, with each block ring having a width of 3.2cm thus resulting in a total AFOV of 25.8cm [39]. The NEMA image quality (IQ) phantom with a 4:1 spheres-to-background ratio was scanned and list-mode PET data were acquired for a total of 30min time period. The sparse detector block rings configuration (sparse-mMR) was implemented to the existing Biograph mMR geometry by retrospectively removing from the PET projection data all counts corresponding to detector pair positions associated with at least one even block ring. Thus, the sparse-mMR can be considered as a hypothetical PET scanner where all the even block rings of the original mMR system have been deactivated. Sparse CBM acquisitions of a constant speed were simulated along an axial distance equal to the axial width of two mMR detector block rings (16 detector rings, 6.4cm) to compensate for the discontinuities in the axial sensitivity due to the gaps.

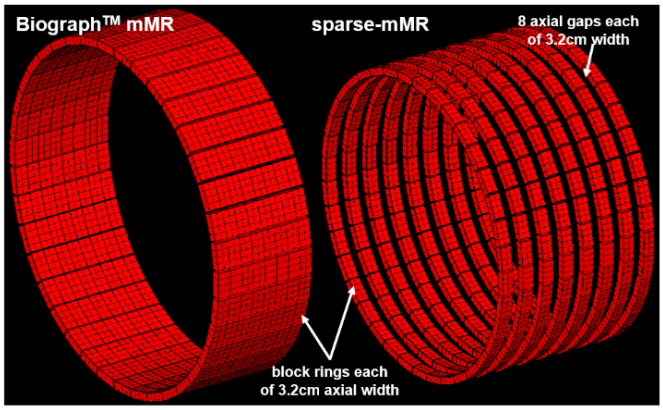

Fig. 1: Visualization of Siemens Biograph™ mMR and sparse-mMR with 8 block rings.

B. Continuous Bed Motion (CBM) PET acquisition with a sparse block rings configuration

The sparse CBM PET acquisitions were simulated by first axially shifting the original stationary mMR projection data by a different number of detector rings each time, from 0 (reference axial position) to 15 to cover an axial translation distance of 2 blocks. Afterwards, all coincidence counts associated with even block rings were removed at each shifted position and the resulting sparse projection PET data were shifted back to the reference initial position 0. This process was iterated 16 times, one for each of the 16 discrete axial steps (0 to 15th) of the scanner bed corresponding to each of the 16 rings encompassed in 2 mMR block rings. The respective output PET data were subsequently added to produce the sparse CBM PET sinogram. The input data for each step was sampled from 16 independent PET list mode data, each corresponding to 16 different scan periods of equal duration.

Sparse-mMR CBM data of ~5, 10, 15 and 20 minutes total scan time were acquired with respective constant CBM speeds of 19, 38, 57 and 76 sec/step (step length=4mm). The respective PET images were evaluated in terms of NEMA contrast recovery (CR) and background variation (BV), against images from stationary 5 min scans using the mMR and a hypothetical compact-½mMR configuration. The latter consisted of only the 4 central mMR block rings.

C. 3D PET system matrix of sparse block rings with extended AFOV due to CBM

The mMR system matrix was considered for the representation of the PET data from all configurations. The gaps in the axially uncompressed (span-1) detector space were accounted before estimating the respective component-based CBM normalization, randoms and scatter correction factors [40]. In Fig. 2, the normalization factors and the prompts sinograms illustrate the sensitivity gaps and the restoration of a smooth continuous counts distribution before and after CBM, respectively.

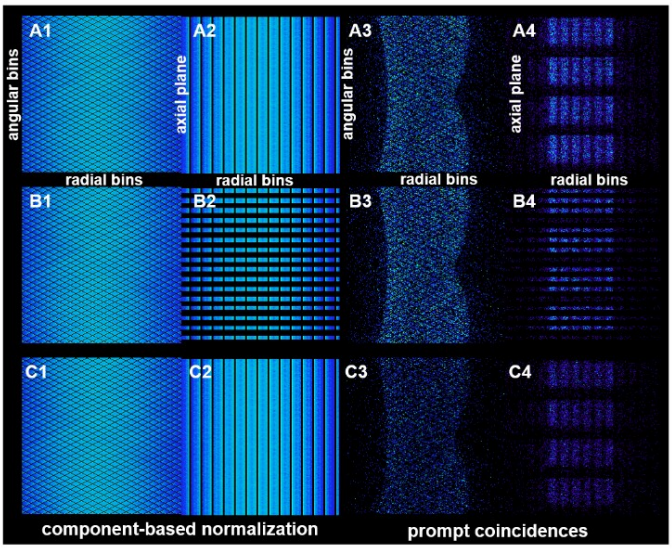

Fig. 2. Two sinogram views of (1st-2nd column) component-based normalization factors and (3rd-4th column) prompts counts from 5min scans, corresponding to (A) the compact-mMR configuration, (B) the sparse-mMR configuration without CBM and (C) the sparse-mMR configuration with CBM mode of 6.4cm bed translation and constant bed speed.

All PET images were reconstructed with the OSEM method (1 iteration, 21 subsets, 4mm FWHM Gaussian post-filtering) using STIR [41].

III. Results

In Fig. 3, we present PET images of the NEMA image quality phantom as reconstructed from data acquired for 5min scans with each of the three configurations. In all images, no artifacts were observed and all spheres were resolved. The CBM mode along an axial distance of 6.4 cm was sufficient to

Authorized licensed use limited to: Cornell University Library. Downloaded on July 21,2020 at 23:57:56 UTC from IEEE Xplore. Restrictions apply.

restore all axial sensitivity discontinuities by evenly acquiring data across all axial planes throughout the gaps. CR differences between the three configurations were within 7% for the 5min scans. BV for the 5min scans increased on average from 4.03% for mMR to 6.80% and 7.60% for the compact-½mMR and sparse-mMR with CBM, respectively. Nevertheless, BV was reduced to 4.16% with the sparse configuration for 20min CBM scans (Fig. 4). In addition, sparse-mMR with CBM attained a smoother axial variation (7.79%) in image noise, relative to compact-½mMR (9.52%).

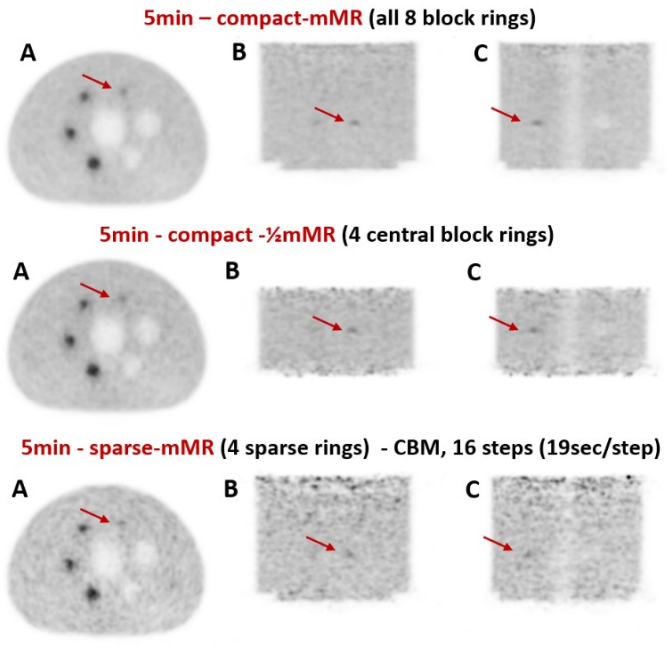

Fig. 3. (A) Transverse, (B) coronal, and (C) sagittal views of 3D PET images of the NEMA image quality phantom reconstructed from 5min list-mode PET scans using (1st row) the compact-mMR and (2nd row) compact ½mMR configurations in stationary acquisition mode and (C) the sparse-mMR configuration in CBM mode with constant bed speed.

IV. Discussion

Our proposal in this work is limited by the constraint of not increasing the current number of detector blocks of modern clinical PET systems and, thus, although it achieves a 100% AFOV extension, the final extended AFOV has a moderate length not exceeding the 60 cm. In this range of AFOV lengths, the redundancy in axial sampling offered by the limited number of detector rings with fully 3D PET acquisitions may only partially compensate for the reduced sensitivity in the axial gap regions between the sparse detector block rings. Thus, in these cases, the CBM PET acquisitions were necessary to complement the redundancy of fully 3D PET scans and together attain the complete recovery of PET image quality and noise smooth variance across the entire AFOV.

For larger AFOV extensions including those involved in total-body PET scanners, the 3D sampling redundancy attained axially by the significantly larger number of block rings required for such configurations may be sufficient to recover the image quality and noise uniformity in the axial gaps interleaved between the block rings without the need for CBM acquisitions. However, these extensions are outside the scope of this work, as they require a larger number of detector blocks than that encompassed in current generation clinical PET systems and thus would have resulted in considerably more expensive PET systems. Nevertheless, the feasibility and premise of the presented concept of fully 3D PET acquisitions with cost-effective sparse block PET detector ring configurations with uniformly interleaved axial gaps between the rings still holds regardless of the AFOV length and the need or not for CBM acquisitions.

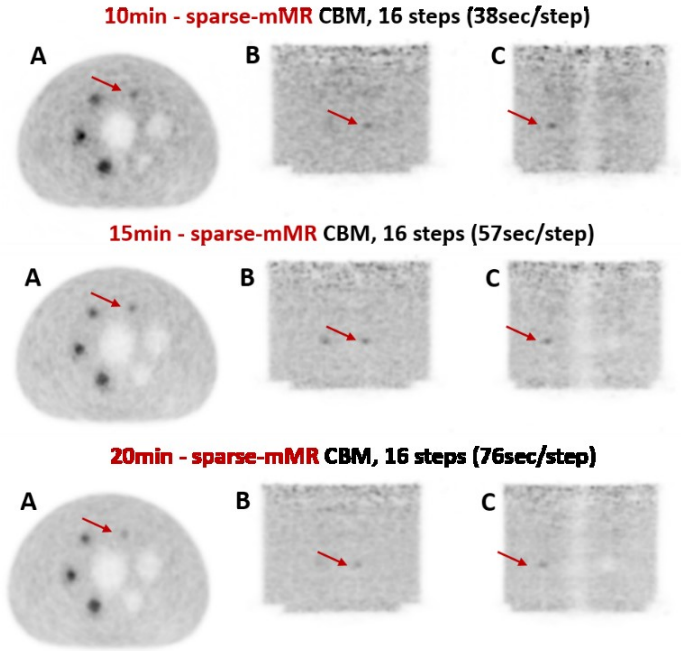

Fig 4. (A) Transverse, (B) coronal, and (C) sagittal views of 3D PET images of the NEMA image quality phantom reconstructed from (1st row) 10 min, (B) 15 min, and (C) 20 min CBM sparse mMR PET list-mode data. The respective CBM speeds are indicated.

This is a proof-of-concept study to demonstrate with real data a cost-effective solution to double the AFOV of current state-of-the-art clinical PET systems by spacing out uniformly the existing block rings or, alternatively, reduce their cost to half by removing the odd or even original block detector rings. As a real mMR system has been used without TOF capabilities, the evaluation was conducted without the benefit of the TOF information which is nowadays supported by the majority of clinical PET scanners with continuously improved time resolutions [42]. We expect that the addition of TOF will improve the image quality and further limit any effects in axial sensitivity due to the axial gaps [43]. Therefore, the current results may indicate the relative performance of the proposed PET geometric configuration under a "worst-case" clinical imaging scenario where TOF information is not available.

Finally, it should be noted that although our current approach of using real scanner data acquisitions and retrospectively removing the counts associated with certain block rings may be convenient for assessing under realistic clinical imaging conditions the performance of the proposed sparse CBM PET scan method, it may not accurately

Authorized licensed use limited to: Cornell University Library. Downloaded on July 21,2020 at 23:57:56 UTC from IEEE Xplore. Restrictions apply.

reproduce the actual performance after physically introducing air gaps between the block rings. Nevertheless, our Monte-Carlo simulation studies that we are conducting in parallel where physical gaps have been implemented have actually reproduced our findings in this study [44, 45].

V. Conclusions

Our findings suggested that CBM could restore continuity in the axial sensitivity profile of PET systems with sparse block rings to achieve similar contrast recovery and smoother noise variation, compared to compact systems, at half the manufacturing cost or double the AFOV. Currently, we continue with the evaluation of the proposed method on previously acquired human mMR PET data.

Acknowledgment

The authors would like to thank Dr. Michael E. Casey for useful discussions regarding technical issues when calculating 3D normalization factors of PET data.

References

[1] H. Zaidi and N. Karakatsanis, "Towards enhanced PET quantification in clinical oncology," *Br J Radiol,* vol. 91, p. 20170508, Jan 2018.

[2] G. K. von Schulthess, "Cost considerations regarding an integrated CT-PET system," *European Radiology,* vol. 10, pp. S377-S380, 2000.

[3] L. Eriksson, D. W. Townsend, M. Conti, C. L. Melcher, M. Eriksson, B. W. Jakoby*, et al.*, "Potentials for large axial field of view positron camera systems," *2008 Ieee Nuclear Science Symposium and Medical Imaging Conference (2008 Nss/Mic), Vols 1-9,* pp. 907-+, 2009.

[4] J. S. Karp, P. E. Kinahan, G. Muehllehner, and P. Countryman, "Effect of Increased Axial-Field of View on the Performance of a Volume Pet Scanner," *Ieee Transactions on Medical Imaging,* vol. 12, pp. 299-306, Jun 1993.

[5] D. W. Townsend, A. Geissbuhler, M. Defrise, E. J. Hoffman, T. J. Spinks, D. L. Bailey*, et al.*, "Fully three-dimensional reconstruction for a PET camera with retractable septa," *IEEE Trans Med Imaging,* vol. 10, pp. 505-12, 1991.

[6] R. Boellaard, A. van Lingen, and A. A. Lammertsma, "Experimental and clinical evaluation of iterative reconstruction (OSEM) in dynamic PET: quantitative characteristics and effects on kinetic modeling," *J Nucl Med,* vol. 42, pp. 808-17, May 2001.

[7] J. T. Thackeray, H. C. Hupe, Y. Wang, J. P. Bankstahl, G. Berding, T. L. Ross*, et al.*, "Myocardial Inflammation Predicts Remodeling and Neuroinflammation After Myocardial Infarction," *Journal of the American College of Cardiology,* vol. 71, pp. 263-275, Jan 23 2018.

[8] K. Tillisch and J. S. Labus, "Advances in Imaging the Brain-Gut Axis: Functional Gastrointestinal Disorders," *Gastroenterology,* vol. 140, pp. 407-U99, Feb 2011.

[9] P. Zanotti-Fregonara, K. Chen, J. S. Liow, M. Fujita, and R. B. Innis, "Image-derived input function for brain PET studies: many challenges and few opportunities," *J Cereb Blood Flow Metab,* vol. 31, pp. 1986-98, Oct 2011.

[10] L. F. de Geus-Oei, E. P. Visser, P. F. Krabbe, B. A. van Hoorn, E. B. Koenders, A. T. Willemsen*, et al.*, "Comparison of image-derived and arterial input functions for estimating the rate of glucose metabolism in therapy-monitoring 18F-FDG PET studies," *J Nucl Med,* vol. 47, pp. 945-9, Jun 2006.

[11] V. Y. Panin, A. M. Smith, J. Hu, F. Kehren, and M. E. Casey, "Continuous bed motion on clinical scanner: design, data correction, and reconstruction," *Physics in Medicine and Biology,* vol. 59, pp. 6153-6174, Oct 21 2014.

[12] N. A. Karakatsanis, M. A. Lodge, A. K. Tahari, Y. Zhou, R. L. Wahl, and A. Rahmim, "Dynamic whole-body PET parametric imaging: I. Concept, acquisition protocol optimization and clinical application," *Physics in Medicine and Biology,* vol. 58, pp. 7391-7418, Oct 21 2013.

[13] N. A. Karakatsanis, M. A. Lodge, Y. Zhou, R. L. Wahl, and A. Rahmim, "Dynamic whole-body PET parametric imaging: II. Task-oriented statistical estimation," *Phys Med Biol,* vol. 58, pp. 7419-45, Oct 21 2013.

[14] N. A. Karakatsanis, M. A. Lodge, Z. Yun, J. Mhlanga, M. A. Chaudhry, A. K. Tahari*, et al.*, "Dynamic multi-bed FDG PET imaging: Feasibility and optimization," *IEEE Nuclear Science Symposium and Medical Imaging Conference (NSS/MIC),* pp. 3863-3870, 23-29 Oct. 2011 2011.

[15] A. Rahmim, M. A. Lodge, N. A. Karakatsanis, V. Y. Panin, Y. Zhou, A. McMillan*, et al.*, "Dynamic whole-body PET imaging: principles, potentials and applications," *European Journal of Nuclear Medicine and Molecular Imaging,* vol. 46, pp. 501-518, Feb 2019.

[16] N. A. Karakatsanis, Y. Zhou, M. A. Lodge, M. E. Casey, R. L. Wahl, and A. Rahmim, "Quantitative whole-body parametric PET imaging incorporating a generalized Patlak model," *2013 Ieee Nuclear Science Symposium and Medical Imaging Conference (Nss/Mic),* 2013.

[17] N. A. Karakatsanis and A. Rahmim, "Whole-body PET parametric imaging employing direct 4D nested reconstruction and a generalized non-linear Patlak model," *Medical Imaging 2014: Physics of Medical Imaging,* vol. 9033, 2014.

[18] N. A. Karakatsanis, M. A. Lodge, A. Rahmim, and H. Zaidi, "Introducing Time-of-Flight and Resolution Recovery Image Reconstruction to Clinical Whole-body PET Parametric Imaging," *2014 Ieee Nuclear Science Symposium and Medical Imaging Conference (Nss/Mic),* 2014.

[19] N. A. Karakatsanis, A. Mehranian, M. A. Lodge, M. E. Casey, A. Rahmim, and H. Zaidi, "Clinical Evaluation of Direct 4D Whole-Body PET Parametric Imaging with Time-of-Flight and Resolution Modeling Capabilities," *2015 Ieee Nuclear Science Symposium and Medical Imaging Conference (Nss/Mic),* 2015.

[20] N. A. Karakatsanis, Y. Zhou, M. A. Lodge, M. E. Casey, R. L. Wahl, H. Zaidi*, et al.*, "Generalized whole-body Patlak parametric imaging for enhanced quantification in clinical PET," *Phys Med Biol,* vol. 60, pp. 8643-73, Nov 21 2015.

[21] N. A. Karakatsanis, M. E. Casey, M. A. Lodge, A. Rahmim, and H. Zaidi, "Whole-body direct 4D parametric PET imaging employing nested generalized Patlak expectation-maximization reconstruction," *Phys Med Biol,* vol. 61, pp. 5456-85, Aug 7 2016.

[22] F. A. Kotasidis, N. A. Karakatsanis, A. Mehranian, and H. Zaidi, "Multi-bed Tracer Kinetic Imaging of Micro-parameters from Dynamic Time-of-flight PET Data," *2015 Ieee Nuclear Science Symposium and Medical Imaging Conference (Nss/Mic),* 2015.

[23] S. R. Cherry, T. Jones, J. S. Karp, J. Y. Qi, W. W. Moses, and R. D. Badawi, "Total-Body PET: Maximizing Sensitivity to Create New Opportunities for Clinical Research and Patient Care," *Journal of Nuclear Medicine,* vol. 59, pp. 3-12, Jan 1 2018.

[24] X. Zhang, Z. Xie, E. Berg, M. S. Judenhofer, W. Liu, T. Xu*, et al.*, "Total-Body Dynamic Reconstruction and Parametric Imaging on the uEXPLORER," *J Nucl Med,* Jul 13 2019.

[25] J. S. Karp, M. J. Geagan, G. Muehllehner, M. E. Werner, T. McDermott, J. P. Schmall*, et al.*, "The PennPET Explorer Scanner for Total Body Applications," *2017 Ieee Nuclear Science Symposium and Medical Imaging Conference (Nss/Mic),* 2017.

[26] J. Karp, J. Schmall, M. Geagan, M. Werner, M. Parma, S. Matej*, et al.*, "Imaging Performance of the PennPET Explorer scanner," *Journal of Nuclear Medicine,* vol. 59, May 1 2018.

[27] J. K. Poon, M. L. Dahlbom, W. W. Moses, K. Balakrishnan, W. L. Wang, S. R. Cherry*, et al.*, "Optimal whole-body PET scanner configurations for different volumes of LSO scintillator: a simulation study," *Physics in Medicine and Biology,* vol. 57, pp. 4077-4094, Jul 7 2012.

[28] S. R. Cherry and J. Czernin, "Discussions with Leaders: A Conversation between Simon Cherry and Johannes Czernin," *Journal of Nuclear Medicine,* vol. 60, pp. 295-298, Mar 1 2019.

[29] M. Conti, "Focus on time-of-flight PET: the benefits of improved time resolution.," *Eur J Nucl Med Mol Imaging,* vol. 38, pp. 1147-1157, 2011.

Authorized licensed use limited to: Cornell University Library. Downloaded on July 21,2020 at 23:57:56 UTC from IEEE Xplore. Restrictions apply.

[30] A. Rahmim, J. Qi, and V. Sossi, "Resolution modeling in PET imaging: Theory, practice, benefits, and pitfalls.," *Med Phys,* vol. 40, pp. 064301-15, 2013.

[31] H. Zaidi and N. Karakatsanis, "Towards enhanced PET quantification in clinical oncology," *British Journal of Radiology,* vol. 91, 2018.

[32] G. Fahrni, N. A. Karakatsanis, G. Di Domenicantonio, V. Garibotto, and H. Zaidi, "Does whole-body Patlak F-18-FDG PET imaging improve lesion detectability in clinical oncology?," *European Radiology,* vol. 29, pp. 4812-4821, Sep 2019.

[33] J. Devriese, L. Beels, E. Deboever, B. Decru, A. Maes, C. Van de Wiele*, et al.*, "Evaluation of FDG PET/CT lesion detectability and quantification harmonization," *European Journal of Nuclear Medicine and Molecular Imaging,* vol. 44, pp. S436-S436, Oct 2017.

[34] C. Lois, B. W. Jakoby, M. J. Long, K. F. Hubner, D. W. Barker, M. E. Casey*, et al.*, "An assessment of the impact of incorporating time-of-flight information into clinical PET/CT imaging.," *J Nucl Med,* vol. 51, pp. 237-245, Feb 2010.

[35] N. A. Karakatsanis, M. A. Lodge, A. Rahmim, and H. Zaidi, "Introducing time-of-flight and resolution recovery image reconstruction to clinical whole-body PET parametric imaging," in *2014 IEEE Nuclear Science Symposium and Medical Imaging Conference (NSS/MIC)*, 2014, pp. 1-6.

[36] T. Yamaya, T. Inaniwa, S. Minohara, E. Yoshida, N. Inadama, F. Nishikido*, et al.*, "A proposal of an open PET geometry," *Phys Med Biol,* vol. 53, pp. 757-73, Feb 7 2008.

[37] N. A. Karakatsanis, S. A. Zein, and S. A. Nehmeh, "Evaluation of Image Quality and Quantitation in a Clinical PET Scanner with a Uniformly Sparse Detector Rings Configuration. ," in *IEEE Nucl Sci Symp Med Imag Conf*, 2018.

[38] J. Zhang, M. I. Knopp, and M. V. Knopp, "Sparse Detector Configuration in SiPM Digital Photon Counting PET: a Feasibility Study," *Mol Imaging Biol,* Aug 9 2018.

[39] G. Delso, S. Furst, B. Jakoby, R. Ladebeck, C. Ganter, S. G. Nekolla*, et al.*, "Performance measurements of the Siemens mMR integrated whole-body PET/MR scanner," *J Nucl Med,* vol. 52, pp. 1914-22, Dec 2011.

[40] M. Casey, H. Gadagkar, and D. Newport, "A component based method for normalization in volume PET," *3rd Int. Meeting on Fully Three-Dimensional Image Reconstruction in Radiology and Nuclear Medicine (Aix-les-Bains, France)* pp. 67-71, 1996.

[41] K. Thielemans, C. Tsoumpas, S. Mustafovic, T. Beisel, P. Aguiar, N. Dikaios*, et al.*, "STIR: software for tomographic image reconstruction release 2.," *Phys Med Biol,* vol. 57, pp. 867-883, Feb 21 2012.

[42] P. Lecoq, "Pushing the Limits in Time-of-Flight PET Imaging," *Ieee Transactions on Radiation and Plasma Medical Sciences,* vol. 1, pp. 473-485, Nov 2017.

[43] M. Conti, "Focus on time-of-flight PET: the benefits of improved time resolution," *European Journal of Nuclear Medicine and Molecular Imaging,* vol. 38, pp. 1147-1157, Jun 2011.

[44] S. Zein, N. Karakatsanis, M. Issa, A. Haj-Ali, and S. Nehmeh, "Performance evaluation of a sparse detector rings PET scanner with extended axial field of view," *Journal of Nuclear Medicine,* vol. 60, May 1 2019.

[45] S. Zein, N. A. Karakatsanis, A. Gupta, J. R. Osborne, and S. A. Nehmeh, "Physical Performance of a PET Scanner Prototype with Extended Axial Field of View using Sparse Detector Module Rings Configuration: A Monte Carlo simulation study," *European Journal of Nuclear Medicine and Molecular Imaging,* vol. 46, pp. S809-S809, Oct 2019.

Authorized licensed use limited to: Cornell University Library. Downloaded on July 21,2020 at 23:57:56 UTC from IEEE Xplore. Restrictions apply.